

THE POLAR CAP STRUCTURE OF THE X-RAY PULSAR 4U 1538–52

T. BULIK,¹ P. MÉSZÁROS,^{1,2} J. W. WOO,³ F. NAGASE,⁴ AND K. MAKISHIMA⁵

Received 1991 November 19; accepted 1992 February 25

ABSTRACT

We have compared the pulse phase-dependent spectral observations of 4U 1538–52 obtained from *Ginga* to a series of static model atmospheres of curved accreting polar caps, utilizing a magnetized radiative transfer code with relativistic polarized cross sections. A χ^2 fit was performed on the symmetrized pulse shapes, allowing the parameters of the two polar caps to vary independently. We find evidence for a significant difference between the caps, both in terms of opening angle and temperature, while the optical depth is similar and compatible with radiative deceleration models. The polar caps appear larger than what is usually estimated from dipole fields, and are not located at the antipodes of each other. A broader distribution of magnetic fields is required than expected from a dipolar field at constant radius. If the magnetic field is indeed dipolar, it should be off-center in respect to the star and the accretion shock height exhibits an unusual dependence on the polar angle. An alternative possibility is that the magnetic field is disordered on scales small compared to the polar cap radius.

Subject headings: pulsars: individual (4U 1538–52) — X-rays: stars

1. INTRODUCTION

The accreting X-ray pulsar 4U 1538–52 is one of a growing number of sources for which excellent phase spectroscopic information has become available in recent years over a broad range of energies, with sufficient spectral resolution to study not only pulse shapes but also the phase variation of cyclotron lines and other features. This object has a relatively long spin period of 530 s, an orbital period of 3.73 days determined from its Doppler modulation and eclipses, and its X-ray luminosity is estimated to be 4×10^{36} ergs s⁻¹ (e.g., Nagase 1989). It is in a massive binary system with a $17 M_{\odot}$ companion of radius $R = 15 R_{\odot}$ and spectral type B0 I at an orbital separation $a = 27 R_{\odot}$, a system somewhat resembling that of Vela X-1, with an orbital plane not far from edge-on as seen by the observer.

Most recently, 4U 1538–52 has been observed with the *Ginga* satellite using the LAC detectors during the period 1988 February 29–March 3, covering a complete cycle of the orbital period. An analysis of these data, separated into eight symmetrized pulse-phase bins, has been presented by Clark et al. (1990), who reported the presence of a cyclotron line around energies of 20 keV, whose profile varied with pulse phase. This was the second instance in which phase-resolved cyclotron line data became available for analysis, the other previous example being Her X-1 (Voges et al. 1982). Previous theoretical calculations of phase-dependent cyclotron line profiles (Mészáros & Nagel 1985a) were able to qualitatively reproduce the Her X-1 behavior, while calculations of the energy dependence of the pulse shapes (e.g., Mészáros & Nagel 1985b; Kii et al. 1986), which used a simplified geometry, provided a limited qualitative comparison with observations. Comparative studies of the

pulse shape morphology of a larger sample of accreting pulsars have been carried out by Wang & Welter (1981), who used simple geometrical beam shapes, and by Leahy (1990), who fitted the data averaged over a broad band of energies to analytical approximations of theoretical pulse shapes, using information accumulated from a variety of previous spacecraft. However, the newer data from *Ginga*, especially on a long-period system such as 4U 1538–52, has significantly better energy and phase resolution, and provides an ideal target for a more detailed comparison of model calculations with observations.

In the present paper we have used the 4U 1538–52 data resolved into 32 phase bins (or 16 when the data is symmetrized about phase 0.5), and have modeled the phase-dependent spectrum using a new set of calculations designed specifically for performing a detailed fit to the observations. We have introduced a number of geometrical features into the analysis, with the purpose of determining the structure of the magnetic field in the polar caps, as well as the inclination angles, the optical depth, and the temperature of the emission regions, allowing for the curvature and for possible differences between the two polar caps, as well as for possible departures from a simple dipole structure. The purpose is to submit the theoretically calculated accretion column models to a first detailed observational test, and conversely, to submit an observationally well-investigated accreting pulsar to a detailed model analysis with the aim to determine as far as possible its geometric structure, field configuration, and relevant plasma parameters. In § 2 we describe the model calculations employed in the analysis. Section 3 gives the details of the procedure used for fitting the models to the observations. The results of the fits of various different models are listed in § 4, and the significance of these results are discussed critically in § 5.

2. ATMOSPHERE MODELS

Because of the relatively low luminosity, we make the approximation of ignoring the effects of scattering by the incoming material above the polar caps and assume that the

¹ Pennsylvania State University, 525 Davey Laboratory, University Park, PA 16802.

² Also Institute of Astronomy, Cambridge.

³ M.I.T., Center for Space Research, 37-611, Cambridge, MA 02139.

⁴ Institute of Space and Astronautical Sciences, 3-1-1 Yoshinodai, Sagamihara, Kanagawa, Japan.

⁵ University of Tokyo, Department of Physics, 1-7-3 Hongo, Bunkyo-ku, Japan.

radiation arises in the surface layers of the polar cap surface. We use therefore individual cap surface elements which are taken to be plane parallel slab models similar to that of Mészáros & Nagel (1985a), with the magnetic field parallel to the local surface normal. However, instead of using nonrelativistic cross sections as in that reference, we use here the fully relativistic cross sections discussed by Alexander & Mészáros (1991a) (cf. also Harding & Daugherty 1991). The main radiative processes are Compton scattering and bremsstrahlung, which in the strong magnetic field of pulsars include both a continuum component and resonant components near the multiples of the cyclotron energy $\hbar\omega_c = 11.2B_{12}$ keV. As in the above reference, we include in the cross sections the effects of radiative damping, plasma and vacuum polarizability, and Doppler dispersion assuming a one-dimensional Maxwellian distribution along the magnetic field, characterized by a parallel electron temperature T_e .

The temperature, density, and magnetic field strength are assumed to be independent of depth in each surface element individually. This is mainly for practical reasons: the search for a fit over a large region of parameter space in T , ρ , B would become unwieldy due to the increase of arbitrary parameters, if one introduced also depth variations of these quantities. This approximation is motivated also by the fact that an inhomogeneous atmosphere can often be considered to have its spectrum determined mainly within a certain range of the depth coordinate, and such a layer may be approximated by homogeneous conditions. The homogeneous atmosphere that we fit is, in this sense, a “surrogate” atmosphere that behaves, for observational purposes, as the inhomogeneous atmosphere. In an accreting pulsar the temperature of the atmosphere is maintained, on average, at a steady state value by the heating from the infalling particles (via binary collisions or collective effects) in balance with the radiative cooling. Without inquiring into the nature and details of the heating, we assume that it balances the radiative losses, and our fitting procedure provides the average temperature, density, and optical depth of a homogeneous atmosphere which provides such radiative losses, with a spectrum and luminosity as observed.

The top boundary condition of this atmosphere is assumed to be free escape. The bottom boundary condition was taken to be one of perfect reflection, compatible with the assumption that the character of the spectrum is determined by the conditions in the slab. Each photon reaching the bottom boundary was simply assumed to be reflected with the same frequency, polarization, and angle it had before reflection. Physically, this is an approximation which is convenient since it does not introduce further additional model parameters related to the conditions below the hot slab. An additional source of soft photons was also investigated, with blackbody spectra of $kT = 0.5$ – 3 keV and adjustable total flux, which can be useful in fitting the low-energy spectrum as found in previous work by Mészáros & Nagel (1985a) and Burnard, Klein, & Arons (1991). However, the fits discussed in this paper do not include this soft flux contribution.

The phase dependence of the spectrum is modeled by calculating the individual cap element atmospheres (each cap being made up of 40 cap elements) with a linear Feautrier radiative transfer code with 32 frequencies, eight angles, and two normal polarization modes. The fluxes shown in the figures are the total fluxes, which are the sum of the two normal mode polarizations, and represent an integration over all the cap elements of each cap. The spectrum is computed in detail over the entire

continuum and the first cyclotron harmonic, with allowance for second harmonic effects. Photons are mainly generated by bremsstrahlung, both in the continuum and at the cyclotron energy. The latter process corresponds to collisions taking an electron up to the first excited level, from which it deexcites radiatively. The first harmonic is dominated by the magnetic resonant scattering of first harmonic photons; these scatter a large number of times before escaping from the wings, due to the very high optical depth near the first harmonic line core. The second harmonic effects play here a somewhat different role than they do in gamma-ray bursters. The second harmonic effects are more important in gamma-ray bursters (e.g., Wang et al. 1989; Alexander & Mészáros 1989), because of the strong power-law continuum at high energies that excite the second harmonic, followed by decay into two first harmonic photons (two-photon scattering, or photon spawning) that can “refill” partially the first harmonic through. However, in accreting pulsars, the high-energy continuum has a thermal dropoff which provides fewer photons at the energy of the second harmonic. As a result, the photon spawning process is much less important in filling the first harmonic as it is in gamma-ray bursters (see, e.g., Figs. 1 and 2 of Alexander & Mészáros 1991b). For the fit temperatures encountered here ($kT \sim 4$ – 5 keV), the depth of the first harmonic varies by $\lesssim 5\%$ when the second harmonic is included in detail as a two-photon scattering (photon spawning) process or when it is treated as simply a single-photon scattering process. With the usual voltage setting of the LAC detector, as used in the observations of 4U 1538–52 modeled here, the second harmonic falls outside the detector response range. However, as pointed out by Clark et al. (1990), the effects of a second harmonic can be important in determining the drop-off at high energies above the shoulder of the first harmonic. This drop-off occurs for 4U 1538–52 at energies where the data starts to merge with the noise, and this part of the spectrum was modeled by including in the detailed spectrum the effects of a generic second harmonic line profile derived from two-photon scattering calculations for the plasma parameters of the atmosphere, whose depth matches the high-energy drop-off.

The physics of the line and continuum spectrum formation is similar to that described in Mészáros & Nagel (1985a, b). The resulting spectra are however qualitatively different, in that the fully relativistic cross sections used here lead to a stronger resonance of the ordinary mode, so that the line is more well defined than in the nonrelativistic limit used there (e.g., Alexander, Mészáros, & Bussard 1989). We calculated the angle-dependent spectra of a series of models with varying magnetic fields of cyclotron energy $16 \text{ keV} \leq \hbar\omega_c \leq 26 \text{ keV}$, and temperatures in the range $3 \leq kT_e \leq 6 \text{ keV}$, which cover the range where acceptable fits were obtained. The density was taken to be $\rho \sim 1 \text{ g cm}^{-3}$, while the Thomson scattering optical depth of the atmosphere was taken to be in the range $5 \leq \tau_T \leq 50$, where the lower limit is somewhat below the typical depth of a radiation-decelerated shock, and the upper corresponds to the typical depth of a nuclear collision decelerated model, which is the extreme value for the low-luminosity Coulomb stopping case (Harding et al. 1984; Miller, Wasserman, & Salpeter 1989).

3. FITTING PROCEDURE

The quality of the data is sufficiently high that it appeared worthwhile to allow for a greater generality of the geometry of the emission regions than is common in this type of analysis.

We took the angular size of the polar caps to be independently variable, i.e., allowed for different sized caps, and allowed the caps to depart from being diametrically opposite (antipodal). We also allowed the possibility of the optical depth, temperature, and magnetic field distribution in each cap to be different. The reasons for adopting such general conditions are, first, that there is no commonly accepted model for the geometry of the emission region, and second, that the present data strongly indicate the need for such conditions, as shown from the fits discussed below. Another generalization (e.g., Leahy 1990) consists of taking into account the curvature of the polar caps, instead of approximating the emission region as a plane slab, which is valid only in the limit of a very small cap size. We assumed the curvature to be spherical, i.e., we did not consider more curved protruding mounds (e.g., Kirk 1985; Burnard et al. 1991); this simplification is justifiable by the low luminosity of 4U 1538–52, indicating that radiation effects should be small. Possible departures from this are discussed in connection with model B in § 3.

Each model was characterized by a set of 13 parameters. These are as follows:

1. α , which is the effective solid angle subtended by the star, i.e., the cross section of the star divided by the distance to the observer.
2. $i_{k\Omega}$, the angle between the wavevector k and the neutron star spin axis Ω .
3. $\Delta\Phi$, the pulse phase lag (modulo 2π) between the phase zero in the model and in the data.
4. $i_{B\Omega}$, the angle between the magnetic axis of each cap and the rotation axis.
5. θ_C , the opening half-angle of the polar cap.
6. T , the temperature of each cap.
7. τ_T , the Thomson optical depth of the cap emission region.
- 8–13. w_{iB} , where $i = 1, \dots, 6$ is a set of six weights for each magnetic field corresponding to values of the ground cyclotron resonances located at 16, 18, 20, 22, 24, and 26 keV (model A), or else the value of the cyclotron energy for six consecutive concentric rings of equal angular width and increasing angular separation centered around the magnetic axis (model B).

The first parameter α and the second parameter ($i_{k\Omega}$) are the same for both caps. The other 11 parameters, however, were allowed in principle to differ between the caps. The magnetic field strengths used above are taken to represent a phenomenological description of the field distribution which need not correspond to any particular physical model such as a dipole, etc. A second, more specific field distribution was also used to test the dipole assumption. A discussion of the implications for specific models is given in § 5.

The theoretical spectra of the individual surface elements used here depend on energy and on the polar angle ψ respect to the local magnetic field direction, taken to be equal to the local surface normal, and they are independent of the local (individual surface element) azimuthal angle φ . The overall cap spectra are also assumed to be independent of the azimuthal angle about the cap symmetry axis. A dependence on the latter can in principle be taken into account, but this complicates significantly the calculations and would involve the introduction of additional arbitrary parameters. Under these assumptions, the polar angles ψ of the individual surface elements can be related to the overall cap polar angle θ respect to the cap symmetry axis, and the latter is related to the pulse phase angle Φ via

$$\cos \theta = \cos i_{k\Omega} \cos i_{B\Omega} + \sin i_{k\Omega} \sin i_{B\Omega} \cos 2\pi\Phi. \quad (1)$$

The flux reaching the observer is given by an integral which implicitly depends on the variable parameters,

$$F(E, \Phi) = \Omega_0 \sum_{\text{caps}} \int d\Omega \cos \psi f_E(\psi) H(\cos \psi), \quad (2)$$

where the sum extends over both polar caps, $\psi = \cos^{-1}(\hat{n} \cdot \hat{k})$ is the angle between the local normal to the star (at the polar coordinates Θ, φ on the surface within the polar cap of opening half-angle Θ_c) and the unit photon wavevector \hat{k} directed toward the observer, Ω_0 is the angular area of the pulsar as seen by the observer, and $H(x)$ is the Heaviside function, $H(x) = (0, 1)$ for $(x < 0, \geq 0)$ which takes into account that radiation is not seen below the local (flat space) horizon. We assume that the magnetic field lines are essentially radial, i.e., we neglect any difference between ψ and the angle θ between the local magnetic field direction B and the observer line-of-sight vector \hat{k} on the surface of the star. The value of the flux at each phase bin was then obtained by linear interpolation from the sum of the theoretical spectra of each visible surface element.

The signal is measured in 48 pulse-height energy channels spanning the range 1–38 keV, with various binning times ranging from 0.5 to 16 s. As in Clark et al., we have ignored the channels 1–20 (energies below 10 keV), where the noise is large. This is not a very serious restriction, as the cyclotron line is well above this lower limit, and it is the line which provides the strongest model constraints on the geometry, e.g., Mészáros & Nagel (1985b). The spectral fitting procedure was carried out by converting the theoretical photon spectra into the count spectra one would have expected to observe with the LAC detectors. The data in this analysis was initially divided into 32 phase bins. The observed pulse shapes in 4U 1538–52 are slightly asymmetric. However, in order to reduce the number of parameters, we performed the model fits on the symmetrized data, made of 16 phase bins which are reflection symmetric about phases 0. and 0.5, where 0. is defined as the center of the main pulse.

The number of photons predicted by the model in each energy channel is calculated by linear interpolation, and converted to counts per channel using the instrumental response function to obtain the expected model counts $f(x_i)$ at each energy channel x_i . The response function of the LAC detectors has been discussed by Makino (1987) and Turner et al. (1989). The observed counts y_i and the estimate of the systematic plus statistical error bars σ_i were then used to calculate the χ^2 statistic,

$$\chi^2 = \sum_{\Phi} \sum_i \left[\frac{y_i - f(x_i)}{\sigma_i} \right]^2, \quad (3)$$

which includes a sum over phases. This quantity should be distributed as a χ^2 distribution whose number of degrees of freedom is the number of measured points (channels times phases) minus the number of parameters. This χ^2 quantity was minimized by varying the parameters mentioned above over the grid of models to obtain χ^2_{\min} .

For values of χ^2_{\min} which are taken to be acceptable by comparing its associated probability with some preset confidence level, a second step consists in obtaining the error bars corresponding to 1 σ deviations obtained from varying parameter values in the neighborhood of the best fit, assuming that the quantity $\chi^2 - \chi^2_{\min}$ is itself distributed as a χ^2 distribution with the number of degrees of freedom equal to the number of parameters of the model (Lampton, Margon, & Bowyer 1976).

TABLE 1
MODEL A: LISTING OF PARAMETERS OF THE
LINE REGION FIT

A.			
Parameter	Units	Value	
α	sr	$1.00 \pm 0.04 * 10^{-30}$	
$i_{k\Omega}$	rad	1.68 ± 0.03	
B.			
Parameter	Units	Main Pulse Cap	Interpulse Cap
$i_{B\Omega}$	rad	0.495 ± 0.04	0.224 ± 0.02
θ_C	rad	0.259 ± 0.01	0.288 ± 0.01
T	keV	4.57 ± 0.15	4.00 ± 0.08
$\log(\tau/7)$	No	-0.097 ± 0.05	-0.067 ± 0.04
16 keV	%	4.7	0.0
18 keV	%	10.8	12.3
20 keV	%	21.9	14.1
22 keV	%	0.0	0.0
24 keV	%	0.0	73.6
26 keV	%	62.6	0.0

To do this, we assume that the form of the χ^2 function around the minimum can be expanded to second order as a function of the parameters as

$$\chi^2(p_i) - \chi_{\min}^2 = \sum_i a_i p_i^2 + \sum_{i,j} b_{ij} p_i p_j. \quad (4)$$

The coefficients a_i and b_{ij} are expressed as numerical derivatives of χ^2 with respect to the parameters. Knowing the values of $\chi^2(p_i) - \chi_{\min}^2$ for a given confidence level, we express parameter p_k as a function of all other parameters, and maximize numerically p_k . These confidence levels were later checked with actual values of χ^2 . The 1σ error bars are shown in Tables 1, 2, 3, and 4.

4. RESULTS

In the following section the values of χ^2 quoted are the reduced values, i.e., χ^2 divided by the number of degrees of freedom. The models were fitted to the data from 10 to 38 keV

TABLE 2
MODEL A: LISTING OF PARAMETERS OF THE
LINE AND CONTINUUM FIT

A.			
Parameter	Units	Value	
α	sr	$0.76 \pm 0.04 * 10^{-30}$	
$i_{k\Omega}$	rad	1.60 ± 0.02	
B.			
Parameter	Units	Main Pulse Cap	Interpulse Cap
$i_{B\Omega}$	rad	0.41 ± 0.02	0.26 ± 0.02
θ_C	rad	0.23 ± 0.01	0.331 ± 0.008
T	keV	5.14 ± 0.11	4.00 ± 0.06
$\log(\tau/7)$	No	-0.008 ± 0.03	-0.012 ± 0.012
16 keV	%	13.8	4.4
18 keV	%	0.0	0.0
20 keV	%	23.8	21.0
22 keV	%	0.0	3.6
24 keV	%	0.0	70.9
26 keV	%	62.3	0.0

TABLE 3
MODEL B: LISTING OF PARAMETERS OF THE
LINE REGION FIT

A.			
Parameter	Units	Value	
α	sr	$0.79 \pm 0.04 * 10^{-30}$	
$i_{k\Omega}$	rad	1.60 ± 0.04	
B.			
Parameter	Units	Main Pulse Cap	Interpulse Cap
$i_{B\Omega}$	rad	0.39 ± 0.03	0.265 ± 0.03
θ_C	rad	0.23 ± 0.01	0.34 ± 0.02
T	keV	5.28 ± 0.16	3.97 ± 0.10
$\log(\tau/7)$	No	-0.08 ± 0.04	-0.11 ± 0.07
Ring 1	keV	21.6	16.4
Ring 2	keV	25.9	25.0
Ring 3	keV	25.9	24.2
Ring 4	keV	26.0+	20.0
Ring 5	keV	18.0	24.2
Ring 6	keV	25.7	22.8

(Ginga channels 20–48), referred to as the whole range, or else to the data from 18 to 38 keV, referred to as the line region (actually, the region above the red wing of the ground cyclotron harmonic). The reason for considering these two ranges separately is that the χ^2 values are generally better for the more restricted, line region.

A number of different models were tried, in order to find the set of parameters that eventually led to a satisfactory fit. The first and simplest model that was tried consisted of two identical small accretion caps (flat, no curvature effects), situated diametrically opposite to each other. The parameters for this were α , the normalization factor; $i_{k\Omega}$, the angle between the direction to observer and the spin axis; $i_{B\Omega}$, the angle between magnetic axis and spin axis; T , the temperature of the caps; and B , the magnetic field. The best reduced χ^2 obtained for this model was very poor, ~ 20 . There are several problems with this simplest model that cause this poor fit. The most significant is that the cyclotron line predicted by a simple model with

TABLE 4
MODEL B: LISTING OF PARAMETERS OF THE
LINE + CONTINUUM FIT

A.			
Parameter	Units	Value	
α	sr	$0.79 \pm 0.03 * 10^{-30}$	
$i_{k\Omega}$	rad	1.60 ± 0.02	
B.			
Parameter	Units	Main Pulse Cap	Interpulse Cap
$i_{B\Omega}$	rad	0.377 ± 0.02	0.262 ± 0.02
θ_C	rad	0.233 ± 0.01	0.339 ± 0.01
T	keV	5.29 ± 0.12	3.96 ± 0.06
$\log(\tau/7)$	No	-0.010 ± 0.02	-0.09 ± 0.05
Ring 1	keV	21.8	16.4
Ring 2	keV	25.9	25.3
Ring 3	keV	25.9	24.4
Ring 4	keV	26.0+	20.0
Ring 5	keV	18.0	24.0
Ring 6	keV	25.7	22.9

a single magnetic field value is much deeper than that shown in the observations of 4U 1538–52. This can be seen, e.g., from the calculations of Alexander & Mészáros (1991b) for one angle; here we use eight angles, but even so the single field theoretical line profiles are unable to match the observed width of the lines. Several possible solutions offer themselves to solve this discrepancy. There could be another component providing some background radiation, which would fill the line. The radiation could have been reprocessed by material around the neutron star. Finally, the structure of the accreting cap might not be simple, i.e., a distribution of fields might be involved. After investigating these possibilities and performing further fits, the largest improvement was obtained with the assumption that the magnetic field is not uniform but has a certain distribution.

The next model used the same assumptions as above, with the exception that the observed spectrum was fitted by a linear combination of several model spectra with magnetic fields in the 16–26 keV range, consisting of a combination of six spectra with cyclotron ground energy increasing in steps of 2 keV. The parameters were the weights in the linear combination of the spectra. The further assumption was also made that the structure of the magnetic field is distributed over much smaller scales than the size of the emitting region. With this field distribution, the fits were considerably improved, but still not to a satisfactory level. Further improvements could be achieved, however, by performing separate fits to each polar cap (or to pulse and interpulse separately), indicating that the two caps may be different.

Models with two different polar caps were then investigated, characterized by two different angles $i_{B\Omega}$ for each cap and a pulse phase lag $\Delta\Phi$ between the two caps (see Fig. 1). Since the data were symmetrized, one can expect the pulse lag to be smaller than $2\pi/16$ which is the interval between consecutive observations. With these assumptions, the reduced value went down to $\chi^2 \sim 7$, a definite improvement, although still too

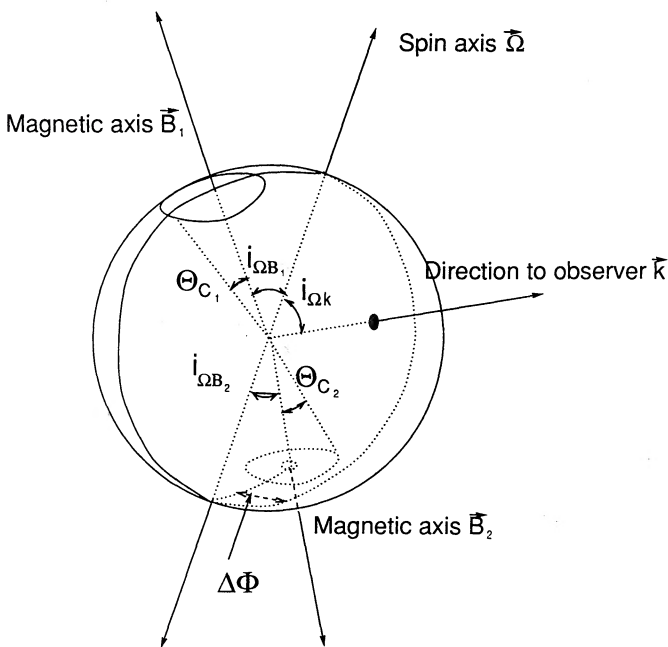


FIG. 1.—Geometrical sketch of the angles involved in the model

large. The bulk of the discrepancy between the data and the model was in this case due to the phase values corresponding to the transition from pulse to interpulse, when the emitting regions are viewed close to “edge-on,” at angles close to perpendicular to the surface normal. For these phases, the models predicted roughly 7–10 times smaller fluxes than the observed ones. The implicit assumption made here is that the cap is small enough that it may be considered to be practically flat, i.e., a simple slab, where the flux naturally tends to zero as one views it sideways. Numerically, one would have expected this to be a good assumption for a calculation with eight discrete polar angles, since under a dipole assumption one typically gets cap opening half-angles of $\lesssim 5^\circ$. If, however, we performed fits with the critical phase angles near “edge-on” omitted, it was possible to get reduced $\chi^2 \sim 1.9$. The most straightforward interpretation of this is that the emitting regions cannot be treated as being small. Indeed, the fits indicate a cap opening half-angle significantly larger than that inferred from the simple dipole assumption (see § 5).

Based on the previous results, models were considered where the polar cap curvature was taken explicitly into account, where the caps can be of different size and need not be located diametrically opposite, and each has its own magnetic field distribution. It was assumed that the caps are circular, characterized by an angular radius θ_c , and that to a first approximation they have spherical curvature. The integration of the flux from each cap was performed using a 40 point grid (four θ points and 10 φ points). The first version of this model, labeled model A, assumes that the spatial scale on which the magnetic field varies is smaller than the size of each integration element. That is, the field distribution is disorganized, in the sense that it does not depend on the polar coordinates. Thus the flux from each of those elements was calculated as combination of the spectra described above. With these assumptions, separate fits were done for the line region 18–38 keV, i.e., *Ginga* channels 26–48, and for the entire region including the low-energy continuum, 10–38 keV, i.e., *Ginga* channels 20–48. The fit to the line region is quite good, the reduced value being $\chi^2 = 1.11$; see Figure 2b. The reduced value for the entire frequency region is not as good, being $\chi^2 = 1.96$; see Figure 2a. This may be an indication that there is another flux component contributing to the formation of the continuum, e.g., a soft photon input, or hot gas emission from the neighborhood of the star. The magnetic field distribution for this model is shown in Figure 3 for each cap separately. These results appear satisfactory, in particular the line region fits, which provide agreement with the data at the 95% confidence level. The best fit parameters to the data for this model are presented in Tables 1 and 2, including error bars computed following the procedure described near the end of the previous section.

We also performed fits to the data using a more common assumption for the magnetic field distribution, labeled model B. In this model the magnetic field was taken to depend on the angular distance from the center of each accretion cap, with no dependence on the azimuth. Each cap was divided into six concentric rings of equal angular size, and the magnetic field value was fitted in each of them. The fit was done both for the 16–38 keV line region, giving a reduced $\chi^2 = 1.48$, and for the entire continuum plus line region 10–38 keV, giving $\chi^2 = 2.11$. These χ^2 values are comparable, although somewhat worse than those for the previous disorganized field case. The magnetic field distribution for the θ -dependent model B is shown in Figure 4.

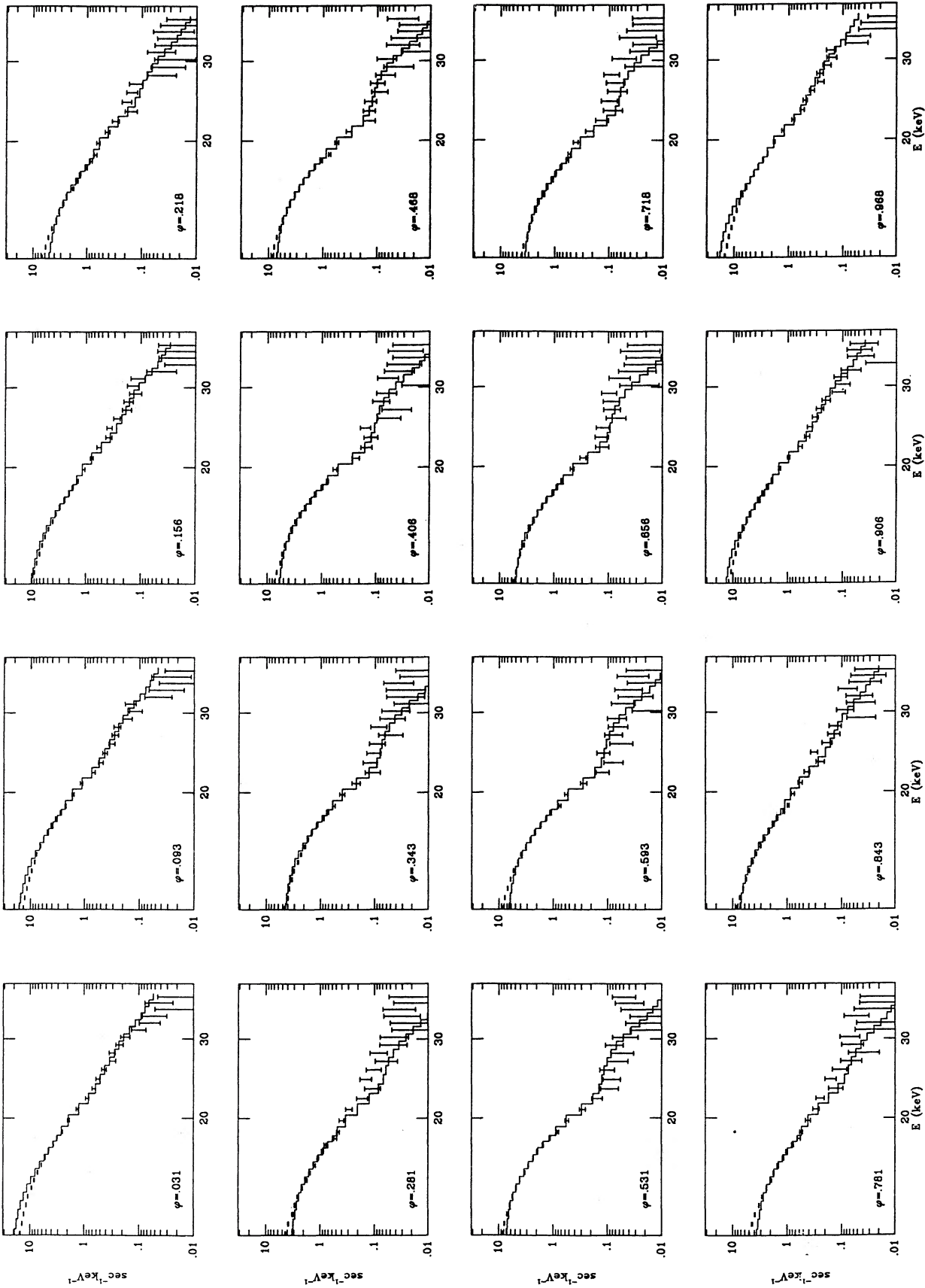


FIG. 2a

FIG. 2.—Comparison of the data with the model spectra of the fit for the 16 phase bins. (a) Results of the fit for 16–38 keV (line region). (b) Results of the fit for the 10–38 keV region (line plus continuum).

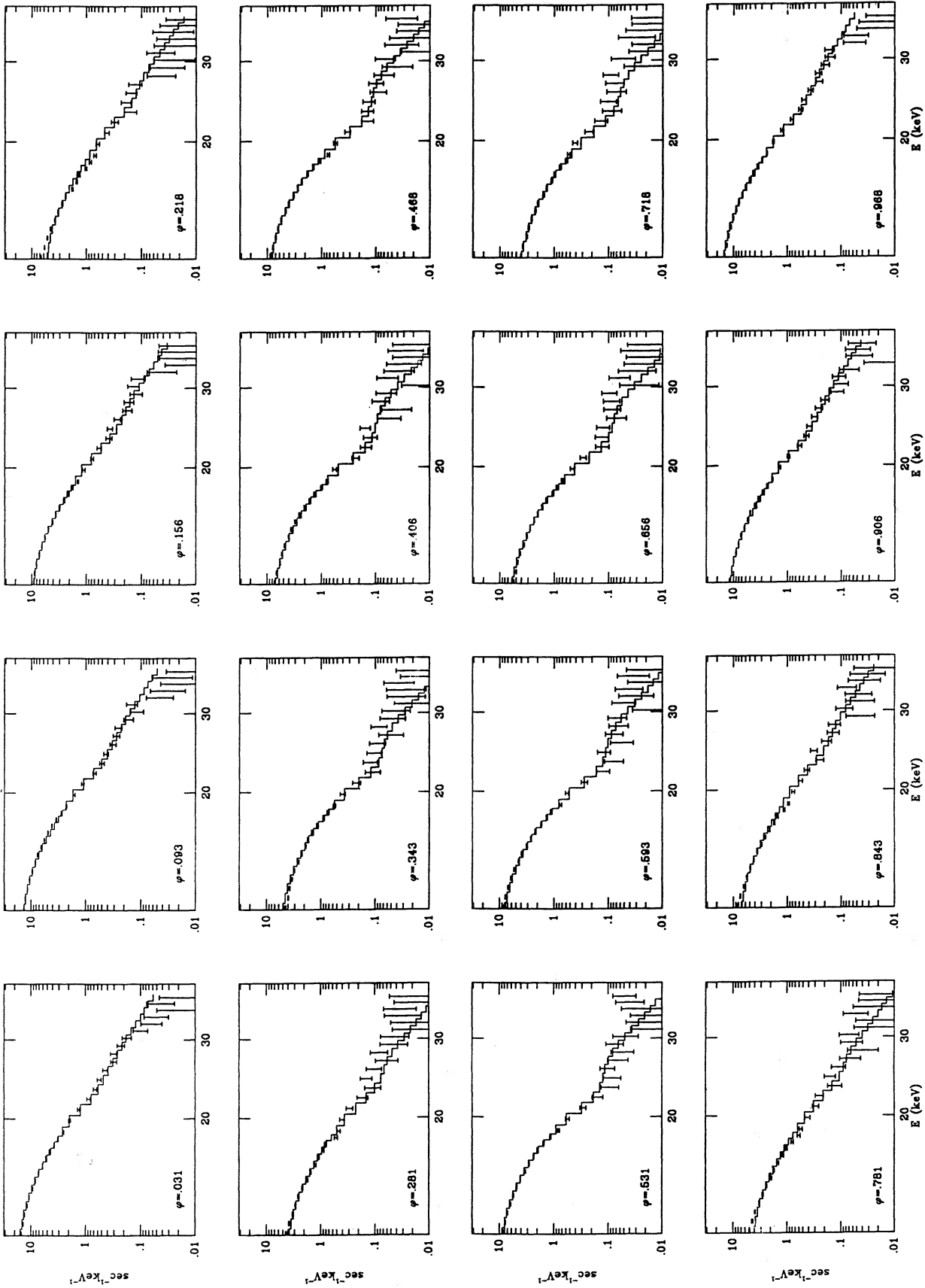


FIG. 2b

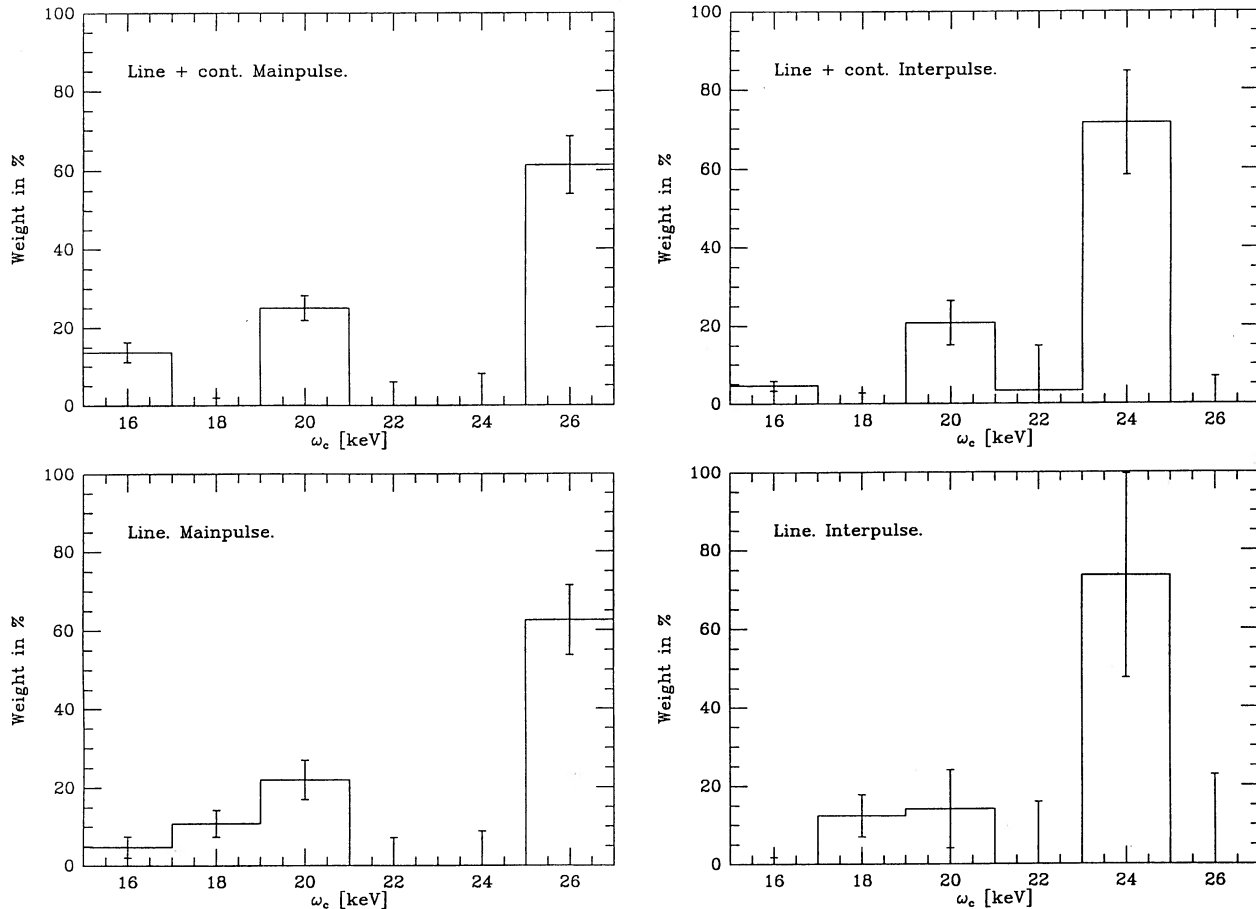


FIG. 3.—The distribution of the magnetic field values in the case where the length scale of the field variation is small compared to the cap size (model A)

5. DISCUSSION

The fits for the last two models (A and B) obtained in the previous section are satisfactory, particularly those concerning the line region 16–38 keV, in the sense that the χ^2 test indicates a reasonable probability for the agreement between the data and the models not to be due to chance. A theoretical interpretation can be given in terms of what one knows about the properties of various calculated models, with a proper awareness of the strengths and limitations imposed by the assumptions inherent in them. In general, none of the currently calculated models is as detailed as the properties of the data discussed here would warrant. The reason is of course the difficulty in dealing simultaneously with the hydrodynamics and the magnetized transfer in the nongray case. The former is usually dealt with in the gray approximation, while the latter is usually dealt with in the static approximation, and none of the calculations has envisaged significant departures from a global dipole symmetry. Nonetheless, it is reasonable to consider the theoretical models as limiting cases whose usefulness extends within certain ranges of parameter space, and whose geometrically simple structure may be used to represent the elements of geometrically more complicated emission regions, as considered here.

The basic model used to describe the data is a magnetized pencil beam model. Such a model has been found to fit the observations of Her X-1, based on the fact that the cyclotron line energy decreases with increasing phase, whereas for fan

beams, it would increase (see Mészáros & Nagel 1985a). A pencil beam is also necessary to explain the pulse shapes and widths. In the case of 4U 1538–52, the same behavior of line energy with phase is found by Clark et al. (1990). We have repeated this analysis here with greater phase resolution, and with our detailed transfer line profile models, rather than Gaussian shapes, and find a qualitatively similar result (see Table 5). Ignoring possible general relativistic effects (e.g., Mészáros & Riffert 1988), the flat space transfer results and the observed line energy behavior indicate therefore that a pencil beam configuration is appropriate for 4U 1538–52. This qualitative agreement between predicted and observed behavior also serves to support the approximate validity of another approximation made, namely that static models provide a useful first-order description of the emission region. This is reasonable behind a radiation or collisionless shock, where bulk motions would be subsonic, and at the low accretion rates in this source ($L_x \lesssim 4 \times 10^{36}$ ergs s^{-1}), one does not expect much scattering in the free-fall region. Consistent with the neglect of mass motions, we have also neglected special relativistic aberration effects, which could lead to the presence of a ring of soft emission around the base of the accretion column (e.g., Brainerd & Mészáros 1991). In a second approximation, these effects would play some role in determining the beam and the effective cap size, but their introduction would undoubtedly greatly increase the complexity of the analysis. In this paper, our aim is to find the first-order departures from the

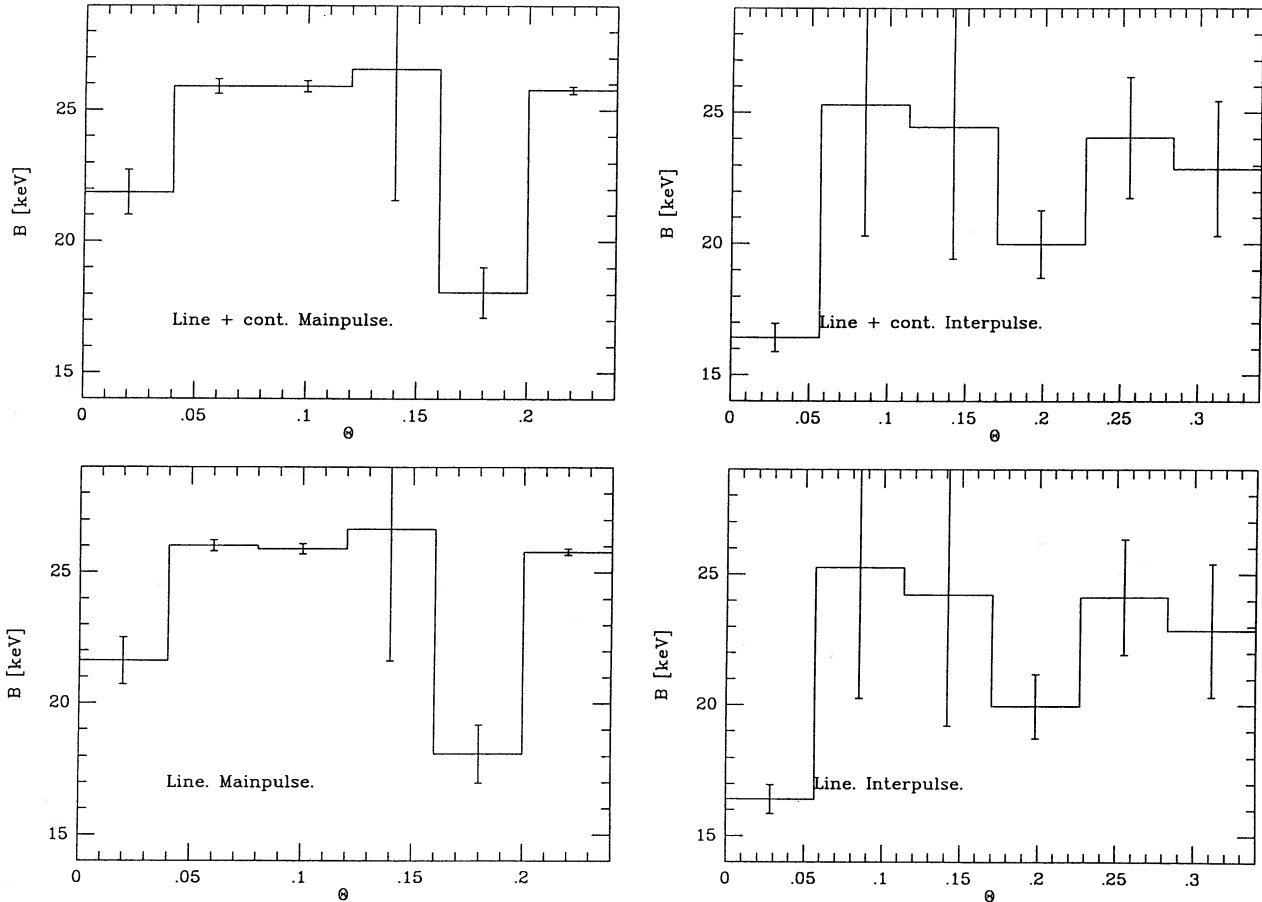


FIG. 4.—The value of the magnetic field as a function of the polar angle measured from the center of the cap (model B). The magnetic field value may be interpreted as being inversely proportional to the height of the emission region.

simplest, commonly used models, for which neglecting these additional complications appears justified.

The optical depth of the emitting region found for model A by the fitting procedure on this pulsar is of order $\tau_T \sim 5.6$ (main pulse cap) and $\tau_T \sim 6.0$ (interpulse cap). The values for model B are similar. This is approximately the value of τ_T

TABLE 5
MODEL A: LINE ENERGY AS A
FUNCTION OF PHASE

Phase	Line Energy (keV)
0.03125	22.31
0.06250	22.29
0.09375	22.25
0.12500	22.18
0.15625	22.08
0.18750	21.96
0.21875	21.85
0.25000	21.73
0.28125	21.62
0.31250	21.54
0.34375	21.47
0.37500	21.41
0.40625	21.36
0.43750	21.32
0.46875	21.30
0.50000	21.29

expected for an accretion shock which is decelerated by radiation pressure (e.g., Basko & Sunyaev 1976; Burnard et al. 1991), and in fact such a value is what was found necessary by Mészáros & Nagel (1985a) in order to fit the spectrum of Her X-1. This opacity is compatible with the fact that the luminosity of 4U 1538–52 is estimated to be $L_x \sim 4 \times 10^{36}$ ergs s^{-1} , which is the critical luminosity estimated by Basko & Sunyaev (1976) for radiation effects to start becoming important.

The temperature values in the emitting region are found to be 4.95 keV (main cap) and 4.0 keV (interpulse cap) for model A, and similar values for model B. These must be interpreted as average values, since lacking a detailed model of the temperature distribution in the shock, it does not make sense to attempt a more detailed fit at the moment. It is, however, interesting that the value of this average temperature is about one-fourth the mean cyclotron ground energy, similar to the values found by fits to the cyclotron line widths in gamma-ray bursters (e.g., Fenimore et al. 1988). The one-fourth value in gamma-ray bursters has been interpreted (Lamb, Wang, & Wasserman 1990) as being compatible with a Compton cooling mechanism. This is seen also from the nonrelativistic Kompaneets equation solution, where the equilibrium Compton temperature is given by $(4kT - \hbar\omega) = 0$ (e.g., Rybicki & Lightman 1979), given that most of the photons interacting with the matter will be cyclotron photons $\hbar\omega_c$, due to the higher resonant cross section.

The cap opening half-angle θ_c found for these models is larger than is typically assumed, being of order 15° , which gives a cap radius $r_c \sim 2.7$ km for a stellar radius of 10 km. By contrast, the usual dipole field expression $\theta^2 \sim 3 \times 10^{-3} L_{37}^{2/7} B_{12}^{-4/7}$, would have predicted an opening half-angle of 1.5° . We stress that the fits indicate the need for a large cap even if one assumes a single field strength, based on geometrical (continuum) flux considerations, i.e., even if we ignore the need to fit the line width with a spread of magnetic fields. This larger cap size implies that cap curvature effects need to be taken into account, as required by the fits. It also implies that there will be a minimum spread in the value of the surface magnetic field value, corresponding to a dipole distribution (which however, is found to be insufficient, see below). We note, however, that a larger cap may still be compatible with matter first approaching along dipole field lines initially headed toward a narrower cap; it may be that along the way matter is redistributed among flux tubes by exchange or other instabilities, which could load dipole lines corresponding to larger polar angles, or perhaps also higher multipolar lines, corresponding to a broader cap at the surface.

The angles made by the rotation axis and the magnetic axes with respect to the line of sight are found, on the basis of the fits, to be fairly large. The rotation axis inclination angle respect to the line of the sight $i_{k\Omega}$ is close to 90° , while the angle between the rotation and magnetic axes is small, $i_{B\Omega} \lesssim 30^\circ$. Thus, the neutron star spin rotation axis is close to the inferred orbital angular momentum axis (which is close to perpendicular to the line of sight, since eclipses are observed), as expected on physical grounds from angular momentum transfer arguments. Also, the magnetic axes are moderately close to perpendicular to the line of sight, although obviously not too close, since there is a detectable pulse modulation. This means that both polar caps are seen, as evident from the presence of an interpulse, and that twice per period they approach a close to edge-on aspect. From the large apparent width of the cyclotron lines, one might naively have expected that the caps would have been seen close to pole-on, which would lead to enhanced Doppler broadening ($\propto \cos \theta$). However, even a maximal pole-on Doppler broadening is unable to fit the line profiles with a single field strength or a dipole distribution at constant radius, and in fact the overall χ^2 fit (including such things as relative continuum and line flux levels as a function of phase) greatly improves as the line of sight makes larger angles to the rotation and magnetic axes.

As mentioned in § 4, various mechanisms were tried to explain the large line broadening, including intrinsic temperature and inclination angle variations, as well as scattering and absorption by an external medium, e.g., by a plasma screen representing the Alfvén surface, an accretion disk or the external medium covering between 4π to smaller fractions of the total solid angle, with various geometries, optical depths, and temperatures. No acceptable fits were found with any of these mechanisms, leaving as the only apparent option that of assuming the presence of a broad magnetic field distribution. In fact, the magnetic field distribution implied by the fits is even broader than that expected from a simple dipole field if one considers only the θ variations along the stellar surface. The latter would lead to a variation of only $\Delta B/B \sim \frac{3}{8} \sin^2 \theta \sim 3\%$, whereas the observed value is about 20%–30%. The additional variation may be explained by a height distribution of the emitting region, which for a dipole field would give a field variation given by $\Delta B/B \sim 3\Delta R/R$. This would require

height variations of $\lesssim 1$ km in order to explain the observed field range. The departure from the simple constant radius geometry is relatively modest, the height to diameter ratio of the cap being $\lesssim 0.2$ for a cap half-angle $\theta_c \sim 0.27$, implying only a mild transgression against the pencil beam assumption (combined pencil and fan beam models could be used, but at this level the increased complexity does not appear warranted). Simple steady state semianalytical calculations with considerable geometrical and microphysical simplifications indicate that one might expect a sort of accretion mound. However, some calculations have envisaged more complicated (e.g., funnel) geometries, while preliminary time-dependent numerical calculations show that there is no guarantee that the shock height should be monotonically decreasing with increasing θ , and that strong instabilities may occur. Lacking strong reasons for preferring some geometries over others, the magnetic field fits were performed with somewhat more generalized assumptions than normally used. This does not rule out the possibility of such simple idealized situations, but allows for other conditions.

One type of fit assumed explicitly an azimuthal symmetry, compatible with our treatment of the pulses in symmetrized form, and assumed that the field strength depends on the polar angle θ . Each polar cap was divided into six concentric rings of equal angular width in θ . The fits performed in this manner (model B) lead to the field distribution shown in Figure 4. If this is interpreted as being due to a dipole field, then the field distribution would translate directly into a height distribution of the emitting matter, since the variations cannot be ascribed to the dipole polar variation at constant height. This would mean that where the field is high, the shock is near the stellar surface, and vice versa. In this case, our calculations only approximate the real situation, since for each ring they assume plane symmetry and neglect any edge effects; as mentioned before, however, the maximum height-to-diameter ratio is less than 20%, so that the departures are not very large. Looking at Figure 4 this interpretation would imply that for the main pulse the shock is closer to the surface near the center, and is higher near the edges of the cap. For the interpulse, the structure is different in detail, although qualitatively it also has a high rim, but it also has a central spike, if this interpretation is correct. The other type of fit that was done (model A) assumed that the field distribution was uncorrelated with θ , that is, that at any point on the cap one might find any of the various field values present. The same distribution was assumed to be valid for all surface elements of the cap, that is, the scale of variation of the field is smaller than the surface integration element (40 per cap). Such a situation might be encountered, e.g., if one had a random or chaotic magnetic field which was frozen in at the time of crystallization of the crust, or if high-order multipoles were present. Some possible scenarios where this might occur could involve thermomagnetic field variations (e.g., as in Blandford, Applegate, & Hernquist 1983), in the presence of a nonuniform heat flux, or perhaps field distortions due to crustal platelet migrations (e.g., Ruderman 1991). In the absence of more qualitative predictions on the possible field configurations, such a small-scale randomness may be a reasonable trial hypothesis. The results for this disorganized model A fit, which is shown in Figure 3, actually gives a somewhat better χ^2 than the more organized model B fits of Figure 4 (which could be compatible with dipole or quadrupole fields). In any case, both from the fits of Figures 3 and 4, one sees the need for a significant fraction of high field ($\hbar\omega_c = 26$ keV) as

well as a less preponderant admixture of somewhat weaker fields ($16 \lesssim h\omega_c \lesssim 20$ keV). Aside from the somewhat better reduced χ^2 value, there seems to be no strong compelling reason to prefer model A over model B, based on these results. The more conventional interpretation of a field varying with the polar angle and/or height (model B, Fig. 4) is at any rate easier to justify, but need not be unique.

Another interesting feature of the fits found here is that they definitely imply a skewness of the magnetic axis, in the sense that the polar cap centers are not located antipodally. Whereas the $\Delta\Phi$ displacement is of the order of the discrete steps in phase angle, i.e., not necessarily significant, the polar displacement θ of one cap respect to the other is indeed significant. This is measured by the different values of the angle $i_{B\Omega}$ between the magnetic axis through the center of each polar cap and the rotation axis Ω , and as seen from the tables, the displacement exceeds three standard deviations. It is not clear from these fits whether one is dealing with a magnetic axis which is bent at the center, or whether it is a more or less straight magnetic axis which is offset from the center of the star. In the latter case, the assumption of radial field lines made here would be worse than in the former case, but the departure from the radial direction would still be less than the finite grid size employed by the calculations, i.e., our calculations would not be expected to be greatly altered at this level of accuracy.

In conclusion, the confrontation of model results with the observations of a well-studied X-ray pulsar presented here is the most detailed to date, and provides the first evidence for the existence of a number of anomalies, for which previously there had been only scattered qualitative evidence. One of these is a noticeable difference in the emission from the two polar caps. Not only are the sizes of the two polar caps noticeably different, they differ also in their temperature, optical

depth, and magnetic field strength distribution. Also, the size deduced for the polar caps is significantly larger than the value deduced for a dipole field, in the Newtonian limit. If future calculations (e.g., including also general relativistic effects) do not drastically modify this conclusion, this could provide information concerning the latching of matter onto field lines at the magnetospheric boundary and near the surface. The model fits also lead to the conclusion that the magnetic field distribution over the polar caps does not agree with a dipole or quadrupole distribution at constant radius, a wider range of magnetic field strengths appearing to be present over relatively small areas. Also the magnetic field does not have an axis of symmetry coincident with a line passing through the stellar center. The axes of magnetic symmetry of the two polar caps meet at an angle whose value departs significantly from zero. Alternatively, if there is a single magnetic axis, this must be considered to be off-center, or bent. The polar cap temperatures are compatible with what one would expect from cyclotron Compton energy balance. The Thomson scattering optical depth of the radiating region is compatible with that expected for a radiation-decelerated shock. If one interprets the magnetic field distribution as being due to a dipole (albeit a skewed, off-center one), and ascribes the field strength variations to height variations of the accretion shock, then the shock varies with polar angle in a nonmonotonical way.

This research has been partially supported through NASA NAGW 1522, NSF AST 8815266 and supercomputing grants from NCSA. T. B. is grateful to the Zaccuche Daniel Foundation, and P. M. is grateful to the Royal Society for support while at the Institute of Astronomy, Cambridge. We thank G. W. Clark for cooperation in the use of the *Ginga* data in this study.

REFERENCES

- Alexander, S. G., & Mészáros, P. 1989, *ApJ*, 344, L1
 ———. 1991a, *ApJ*, 372, 554
 ———. 1991b, *ApJ*, 372, 565
 Alexander, S. G., Mészáros, P., & Bussard, R. W. 1989, *ApJ*, 342, 928
 Basko, M. M., & Sunyaev, R. A. 1976, *MNRAS*, 175, 395
 Blandford, R., Applegate, J., & Hernquist, L. 1983, *MNRAS*, 204, 1025
 Brainerd, J., & Mészáros, P. 1991, *ApJ*, 369, 179
 Burnard, D. J., Klein, R. I., & Arons, J. 1991, 367, 575
 Clark, G. W., et al. 1990, *ApJ*, 353, 274
 Fenimore, E. D., et al. 1988, *ApJ*, 335, L71
 Harding, A. K., & Daugherty, J. 1991, *ApJ*, 374, 687
 Harding, A. K., Mészáros, P., Kirk, J. G., & Galloway, D. 1984, *ApJ*, 278, 369
 Kii, T., et al. 1986, *PASJ*, 38, 751
 Kirk, J. G. 1985, *A&A*, 142, 430
 Lamb, D. Q., Wang, J. C., & Wasserman, I. 1990, *ApJ*, 363, 370
 Lampton, M., Margon, B., & Bowyer, S. 1976, *ApJ*, 208, 177
 Leahy, D. 1990, *MNRAS*, 242, 188
 Makino, F. 1987, *Ap. Letters Comm.*, 25, 223
 Mészáros, P., & Nagel, 1985a, *ApJ*, 298, 147
 ———. 1985b, *ApJ*, 299, 138
 Mészáros, P., & Riffert, H. 1988, *ApJ*, 327, 712
 Miller, G. S., Wasserman, I., & Salpeter, E. E. 1989, *ApJ*, 346, 405
 Nagase, F. 1989, *PASJ*, 41, 1
 Ruderman, M. 1991, *ApJ*, 366, 261
 Rybicki, G., & Lightman, A. P. 1979, *Radiative Processes in Astrophysics* (New York: Wiley)
 Turner, M. J., et al. 1989, *PASJ*, 41, 345
 Voges, W., Pietsch, W., Reppin, C., Trümper, J., Kendziorra, E., & Staubert, R. 1982, *ApJ*, 263, 803
 Wang, J. C., et al. 1989, *Phys. Rev. Lett.*, 63, 1550
 Wang, Y.-M., & Welter, G. L. 1981, *A&A*, 102, 97

Note added in proof.—After this paper had been accepted we received a preprint entitled “Energy-dependent Effects of Scattering Atmosphere on X-Ray Pulsar Pulse Profiles” by S. Sturmer and C. Dermer. The effects discussed in that paper do not apply to 4U 1538 at the energies > 10 keV dealt with here since resonant scattering at $R \approx 2R_*$ would be negligible in this region of the spectrum.